fractal and fractional

MDPI

Article

A Residual Power Series Framework in Fractional Convection–Diffusion Model with Convergence Analysis and Applications

Sajad Iqbal [1], Ilhem Kadri [2], Brij Mohan [3], Manal Y. A. Juma [4] and Nidal E. Taha [4,*]

[1] School of Mathematics, Yangzhou University, Yangzhou 225002, China; sajad_iqbal@ujs.edu.cn
[2] Department of Mathematics, University of Oran 1 Ahmed Ben Bella, Oran 31000, Algeria; kadri.ilhem@univ-oran1.dz
[3] Department of Mathematics, Hansraj College, University of Delhi, Delhi 110007, India; brijmohan@hrc.du.ac.in
[4] Department of Mathematics, College of Science, Qassim University, Buraidah 51452, Saudi Arabia; m.jum@qu.edu.sa
* Correspondence: n.taha@qu.edu.sa

Abstract

This work investigates a novel residual power series technique (RPST) to analyze time-fractional convection–diffusion equations (TFC-DEqs) that model transport processes with memory and anomalous diffusion effects. The approach is appropriate for both linear and nonlinear cases because it avoids linearization, discretizations, and other simplifying assumptions. The reliability of the method is demonstrated by the results, which show strong agreement with exact solutions and rapid convergence as the fractional order approaches one. The error analysis also verifies that such results can be obtained with high accuracy by considering only a few terms, which demonstrates the efficiency of the method. A significant outcome of this research is the development of a reliable and efficient analytical framework that can accommodate complex transport phenomena without resorting to assumptions. The results are significant as they offer insights and show promise for potential applications in engineering and applied science, particularly for nonlocal and memory-dependent systems.

Keywords: residual power series approach; approximate solution; fractional differential equations; nonlinear equations; caputo fractional derivative; convection–diffusion equations

1. Introduction

Fractional calculus (FC) can be traced back to the 17th century when mathematicians like Leibniz and Euler studied the idea of generalizing the derivative and integral orders. Nevertheless, it was in the 19th century when FC was formally established, owing to the efforts of mathematicians like Liouville and Riemann [1–3]. In recent years, FC has gained significant attention because of its potential to model complex systems that display long-range memory effects and anomalous diffusion, as observed in different scientific and technological fields [4]. This mathematical tool has been utilized by researchers to describe complex behaviors that cannot be adequately handled by the usual integer-order integration and differentiation operators, as discussed in [5–7] and the references within. When simulating intricate natural phenomena, FC overcomes the drawbacks of conventional integrals and derivatives [8,9]. According to sources [3,10,11], this mathematical framework has been successful in analyzing a variety of situations across multiple domains by using fractional operators. Recently, Fractional Differential Equations (FDEqs) have

Check for updates

Academic Editors: Libo Feng, Yang Liu and Lin Liu

Received: 2 September 2026
Revised: 16 September 2026
Accepted: 17 September 2026
Published: 20 September 2026

Copyright: © 2026 by the authors. Licensee MDPI, Basel, Switzerland. This article is an open access article distributed under the terms and conditions of the Creative Commons Attribution (CC BY) license.

attracted considerable attention from various researchers due to their increased potential for modeling real-life situations accurately in various domains of engineering and scientific applications [12–14]. Consequently, considerable research has been undertaken to develop effective mathematical theories and analytical approaches for solving FDEs [15–19]. These studies aim to improve the understanding of the dynamics of FDEs and provide accurate predictions of their behavior [20–24]. Related developments have further contributed to the analysis and solution of fractional models [25]. To tackle the challenges associated with FDEqs, various approaches have been proposed to approximate the solutions for FDEqs and their systems [26,27]. Among the notable approaches are the modified Adomian decomposition method (ADM) [28], the fractional variational-iteration method (FVIM) [29,30], and the homotopy perturbation method (HPM) [31–33]. In addition to this, RPST improves the solution of FDEqs incrementally by representing the residual error in power series form. Initially presented in [16], Arqub successfully used RPST to solve fuzzy first-order and second-order DEqs by solving linear equations with one or two variables.

In the years since, the core methodology has experienced crucial algorithmic evolution, focusing extensively on pairing residual computations with custom integral transforms to resolve multidimensional non-linear operator maps [34] as well as adapting power series solutions to generalized α-Caputo formulations without reliance on low-order reductions [35].

RPST stands out for several reasons [19]. Firstly, it does not require coefficient comparison and recursion relations; hence, it is easy to implement. Secondly, it guarantees the convergence of the series by effectively minimizing the residual errors. Thirdly, the methodology is robust to computational rounding errors; hence, it requires minimal memory and computational time. Finally, it elegantly handles the transitions between different orders and nonlinearities; hence, it can be readily applied to problems where a reasonable guess is available. In conclusion, the above methodologies, among other approaches, are useful tools for approximating the solutions to FDEqs and have been successfully implemented for a wide range of linear and nonlinear problems.

The convection–diffusion equation is a useful approach for describing the combined effect of convection and diffusion on the movement of various substances or their properties in a medium. This approach is widely used in many fields related to mass transfer, heat transfer, fluid dynamics, etc. One such scenario that we can relate is that of a river's flow, where the speed of the water helps in transporting substances such as salt. The general formulation of time-fractional convection–diffusion equations (TFC-DEqs) is given by

$$\frac{\partial^{\alpha}\nu}{\partial\tau^{\alpha}} = \nabla\cdot(\mathcal{D}\cdot\nabla\nu) - \nabla\cdot(\vec{u}\nu) + \mathcal{S}, \tag{1}$$

where ν denotes the variable of interest, $\mathcal{D}$ symbolizes the diffusion coefficient (which may refer to mass or thermal diffusion), $\vec{u}$ represents the average velocity of the substance in question, $\mathcal{S}$ serves as the source term for ν, and ∇ indicates the gradient operator.

Before proceeding, it is essential to address the dimensional homogeneity of the fractional governing equations. Due to the nature of the Caputo fractional derivative, the operator $\frac{\partial^{\alpha}}{\partial\tau^{\alpha}}$ carries fractional physical dimensions of $T^{-\alpha}$. To ensure the equations are dimensionally consistent across the entire interval $\alpha \in (0,1]$, we present the governing equations in a non-dimensionalized form.

Let T_c and L_c be the characteristic time and length scales, respectively. We introduce the following dimensionless variables

$$\tau^{*} = \frac{\tau}{T_c}, \quad \zeta^{*} = \frac{\zeta}{L_c}, \quad v^{*} = \frac{v}{V_c},$$

where V_c is the characteristic velocity. Substituting these into the dimensional equations and dropping the asterisks for simplicity, we obtain the dimensionless forms presented in Equations (1) and (7). In this dimensionless framework, the fractional operators and all transport coefficients are treated as dimensionless quantities.

The Caputo sense is employed for defining the fractional derivative in the context of this equation. Extensive research has been conducted on this equation in classical contexts, utilizing a variety of analytical and numerical techniques. Notable methods include the VIM [36], HPM [37], and the Laplace transform HPM [38]. Within the domain of FC, ADM has also been applied [39]. More recently, there has been a significant shift toward modeling specialized transport and solute mechanics under non-linear settings and pushing for structural investigations that balance both fractional operator memory effects and complex advection boundaries [40].

Nevertheless, many of these methods face inherent challenges, such as complex calculations involving He's and Adomian's polynomials for nonlinear terms, divergent results, and considerable computational demands.

While traditional semi-analytical techniques have been extensively implemented to solve fractional differential equations, many face distinct inherent limitations when dealing with complex non-linear structures. A key distinction of the RPST over these established methods lies in its remarkable computational simplicity and direct execution workflow. Specifically, unlike the ADM which requires the intensive and mathematically rigorous computation of Adomian polynomials to handle non-linear operators, RPST bypasses this requirement entirely by evaluating residual errors via a straightforward fractional Taylor series framework. Furthermore, RPST avoids the formulation of He's polynomials, a necessary and often computationally demanding step intrinsic to the HPM. It also stands in contrast to the VIM, as RPST eliminates the need to determine optimal Lagrange multipliers via stationary conditions, completely skipping the corresponding integration steps. By eliminating the need for coefficient comparisons, recursion relations, or intricate polynomial calculations, RPST presents a highly robust, memory-efficient framework that yields rapidly converging and highly accurate analytical descriptions for both linear and non-linear transport models.

Considering the aforementioned problems, this paper proposes an approximate analytical solution for four different types of TFC-DEqs, which include linear and non-linear problems, through the application of the RPST.

Unlike foundational developments and previous applications of the Residual Power Series Technique [16], which focused primarily on linear or lower-order fractional differential equations, the framework developed in this study is specifically tailored to address TFC-DEqs containing both linear and highly nonlinear terms. Furthermore, while many traditional RPST applications rely on numerical comparisons alone to demonstrate accuracy, our approach provides explicit, rigorous mathematical convergence verification uniquely derived for each individual case study. This ensures not only the computational viability of the framework across varied transport conditions but also establishes its formal analytical reliability.

The Caputo fractional derivative is found to be useful for the examination of physical problems, such as TFC-DEqs, as it is efficient in modeling problems that include memory effects and long-range interactions, which are common in such problems. Through the inclusion of the Caputo fractional derivative, a better understanding of the complex problems involved in convection–diffusion problems is possible. The RPST, based on the fractional Taylor series, is recognized as a highly efficient and simple method for the solution of FDEqs compared to other methods, such as HPM and ADM. It is observed that the RPST has faster convergence compared to its peers, which is a major advantage for solving FDEqs.

One of the most interesting characteristics of the RPST is that despite the inclusion of only a few terms in its solutions, a highly accurate solution is possible.

The numerical analysis involves the comparison of the approximate analytical solutions for various values of the fractional order (α), where convergence to the exact solution is quick as the value of α approaches 1. Moreover, the solutions are also presented in tabular form for a more detailed analysis.

The structure of the paper is as follows: Section 2 will discuss the basic definitions and results used in the later discussion. In Section 3, the methodology of the RPST method for solving TFC-DEqs will be discussed. Numerical examples verifying the proposed method are presented in Section 4. Lastly, Section 5 offers conclusive remarks emphasizing the efficacy of the method and presenting a convergence analysis, with Section 6 summarizing the overall conclusions drawn from this study.

2. Essential Concepts of Fractional Calculus

In this section, we outline fundamental concepts that are crucial for understanding the subsequent analysis.

Definition 1 ([7,41]). *The Caputo fractional derivative is defined as*

$$^{C}\mathcal{D}_{\tau}^{\alpha}\Phi(\zeta,\tau) = \mathcal{J}^{n-\alpha}\mathcal{D}_{\tau}^{n}\Phi(\zeta,\tau), \quad n-1 < \alpha \leq n, \tau > 0, \tag{2}$$

where n is the natural number, Γ represents the gamma function and $\mathcal{J}^{\alpha}$ is the fractional integral operator in the Riemann–Liouville sense, defined as

$$\mathcal{J}^{\alpha}\Phi(\zeta,\tau) = \frac{1}{\Gamma(\alpha)}\int_{0}^{\tau}(\tau-\eta)^{\alpha-1}\Phi(\zeta,\eta)d\eta, \quad \alpha,\eta > 0, \tag{3}$$

provided that the integral exists.

The most important properties of the Caputo fractional derivative that are required for further analysis in this study are

1.
$$^{C}\mathcal{D}_{\tau}^{\alpha}(\tau^{\beta}) = \frac{\Gamma(\beta+1)}{\Gamma(\beta-\alpha+1)}\tau^{\beta-\alpha}, \quad \beta > \lceil\alpha\rceil - 1, \ \tau > 0.$$

2.
$$^{C}\mathcal{D}_{\tau}^{\alpha}(c) = 0, \quad \text{for any c} \in \mathbb{R}.$$

For more properties, readers are encouraged to refer to [1–3].

Theorem 1 ([18,20]). *The F-PS $\sum_{n=0}^{\infty} c_n(\tau-\tau_0)^{n\alpha}$ can exhibit one of three possible behaviors regarding converges.*

- *The series converges only for $\tau = \tau_0$;*
- *The series converges only for $\tau \geq \tau_0$;*
- *The series converges for $\tau \in [\tau_0, \tau_0 + r)$, where r represents the radius of convergence, and diverges for $\tau > \tau_0 + r$.*

Definition 2 ([16,18]). *The multiple F-PS about $\tau = \tau_0$ can be expressed in the following form:*

$$\sum_{n=0}^{\infty}\Omega_n(\zeta)(\tau-\tau_0)^{n\alpha} = \Omega_0(\zeta) + \Omega_1(\zeta)(\tau-\tau_0)^{\alpha} + \Omega_2(\zeta)(\tau-\tau_0)^{2\alpha} + \ldots \tag{4}$$

This representation is valid under the conditions $0 \leq m-1 < \alpha \leq m$ *(where* $m \in \mathbb{N}$*) and* $\tau - \tau_0 \geq 0$*. In this context,* $\Omega_n(\zeta)$ *denotes the coefficients of the series, characterizing it as a multiple power series centered at* $\tau = \tau_0$*.*

Theorem 2 ([18,20]). *Assume that* $\nu(\zeta,\tau)$ *has a multiple F-PS representation at* $\tau = \tau_0$ *of the form:*

$$\nu(\zeta,\tau) = \sum_{n=0}^{\infty} \Omega_n(\zeta)(\tau-\tau_0)^{n\alpha}, \quad \tau \in [\tau_0, \tau_0 + r), \quad \zeta \in I. \tag{5}$$

If ${}^{\mathcal{C}}\mathcal{D}_{\tau}^{n\alpha}\nu(\zeta,\tau)$ *are continuous on* $I \times [\tau_0, \tau_0 + r)$ *for* $n = 0, 1, 2, \ldots$*, then the coefficients of the series can be estimated as*

$$\Omega_n(\zeta) = \frac{{}^{\mathcal{C}}\mathcal{D}_{\tau}^{n\alpha}\nu(\zeta,\tau_0)}{\Gamma(1+n\alpha)}, \quad n = 0, 1, 2, \ldots \tag{6}$$

3. Residual Power Series Framework for Fractional Models

This section introduces a comprehensive methodology to solve TFC-DEqs. The problem we aim to solve is described in its general form by the following equations

$${}^{\mathcal{C}}\mathcal{D}_{\tau}^{\alpha}\nu(\zeta,\tau) = \mathbb{L}_{\zeta\zeta}[\nu(\zeta,\tau)] - \mathbb{N}[\nu(\zeta,\tau)] + \Phi(\zeta,\tau), \tag{7}$$

with the initial condition (I.C.)

$$\nu(\zeta,0) = \gamma(\zeta). \tag{8}$$

In this context, $\nu(\zeta,\tau)$ is a function dependent on two variables, while ${}^{\mathcal{C}}\mathcal{D}_{\tau}^{\alpha} = \frac{\partial^{\alpha}}{\partial\tau^{\alpha}}$ indicates the Caputo derivative of order α. Throughout this section, unless otherwise stated, we restrict the fractional parameter α to the interval $0 < \alpha \leq 1$. Consequently, the integer-bound m in Definition 2 is fixed at $m = 1$.

The term $\mathbb{L}_{\zeta\zeta} = \frac{\partial^2}{\partial\zeta^2}$ refers to a linear operator, and $\mathbb{N}$ denotes a non-linear operator. Additionally, $\Phi(\zeta,\tau)$ represents a non-homogeneous term. The RPST formulates the solution to Equation (7) as a fractional power series expansion around the initial point at $\tau = 0$:

$$\nu(\zeta,\tau) = \sum_{n=0}^{\infty} \Omega_n(\zeta)\frac{\tau^{n\alpha}}{\Gamma(1+n\alpha)}, \quad -\infty < \zeta < \infty, \tau \in [0, \mathrm{r}). \tag{9}$$

In the above series expansion, $\Omega_n(\zeta)$ denotes the n-th order coefficient function (or recursive component) of the solution, which depends exclusively on the spatial variable ζ. Since it is easier to deal with a finite series than an infinite series, the truncated series solution of Equation (7) can be denoted $\nu_k(\zeta,\tau)$ and expressed as

$$\nu_k(\zeta,\tau) = \sum_{n=0}^{k} \Omega_n(\zeta)\frac{\tau^{n\alpha}}{\Gamma(1+n\alpha)}. \tag{10}$$

This can be written in an alternative way as

$$\nu_k(\zeta,\tau) = \nu_0(\zeta,\tau) + \sum_{n=1}^{k} \Omega_n(\zeta)\frac{\tau^{n\alpha}}{\Gamma(1+n\alpha)}, \quad k = 1, 2, 3, \ldots \tag{11}$$

Here $\nu_0(\zeta,\tau) = \nu(\zeta,0)$ is the initial approximate solution of $\nu(\zeta,\tau)$. The residual function associated with Equation (7) is described as

$$Res_{\nu(\zeta,\tau)} = {}^{\mathcal{C}}\mathcal{D}_{\tau}^{\alpha}\nu(\zeta,\tau) - \mathbb{L}_{\zeta\zeta}[\nu(\zeta,\tau)] + \mathbb{N}[\nu(\zeta,\tau)] - \Phi(\zeta,\tau). \tag{12}$$

Therefore, the *k-th* residual function can be stated as

$$Res_{\nu,k(\zeta,\tau)} = {}^{\mathcal{C}}\mathcal{D}_{\tau}^{\alpha}\nu_k(\zeta,\tau) - \mathbb{L}_{\zeta\zeta}[\nu_k(\zeta,\tau)] + \mathbb{N}[\nu_k(\zeta,\tau)] - \Phi(\zeta,\tau). \tag{13}$$

To obtain the first approximation, take $k = 1$ in Equations (11) and (13) as

$$\nu_1(\zeta,\tau) = \gamma(\zeta) + \Omega_1(\zeta)\frac{\tau^{\alpha}}{\Gamma(1+\alpha)}, \tag{14}$$

$$Res_{\nu,1} = {}^{\mathcal{C}}\mathcal{D}_{\tau}^{\alpha}\nu_1(\zeta,\tau) - \mathbb{L}_{\zeta\zeta}[\nu_1(\zeta,\tau)] + \mathbb{N}[\nu_1(\zeta,\tau)] - \Phi(\zeta,\tau), \tag{15}$$

and by substituting Equation (14) in Equation (15), the residual function for the first approximation can be obtained as follows:

$$Res_{\nu,1(\zeta,\tau)} = \Omega_1(\zeta) - \mathbb{L}_{\zeta\zeta}[\nu_1(\zeta,\tau)] + \mathbb{N}[\nu_1(\zeta,\tau)] - \Phi(\zeta,\tau). \tag{16}$$

Finally by setting $Res_{\nu,1(\zeta,0)} = 0$ allows us to get

$$\Omega_1(\zeta) = \Phi(\zeta,0) + \mathbb{L}_{\zeta\zeta}[\nu_1(\zeta,0)] - \mathbb{N}[\nu_1(\zeta,0)]. \tag{17}$$

In a similar way, $\Omega_2(\zeta), \Omega_3(\zeta)$, and so forth for $k \geq 2$ can be computed by implementing Equation (11) in Equation (13) and applying the following condition for $k \geq 2$:

$${}^{\mathcal{C}}\mathcal{D}_{\tau}^{(k-1)\alpha} Res_{\nu,k}(\zeta,0) = 0. \tag{18}$$

So, the general recurrence formula for computing the coefficients $g_n(\zeta)$ is given as

$$g_0(\zeta) = v(\zeta,0) = \gamma(\zeta). \tag{19}$$

$$g_n(\zeta) = \left[L_{z\zeta}[\nu_{n-1}] - N[\nu_{n-1}] + \Phi(\zeta,\tau)\right]_{\tau=0}^{(n-1)\alpha}, \qquad n \geq 1. \tag{20}$$

Theorem 3 ([32,42]). *If the initial guess ν_0 is contained inside the ball $\mathcal{B}(\nu, r)$ of the series solution $\nu(\zeta,\tau)$, then the solution of (11) is convergent, whenever there exists an $\epsilon \in (0,1)$ such that $||\nu_{n+1}|| \leq \epsilon||\nu_n||$.*

Remark 1 ([32,42]). *The maximum truncation error of $\nu(\zeta,\tau)$ can be expressed as $\frac{\epsilon^{n+1}}{1-\epsilon}||\nu_0||$, where $\epsilon \in (0,1)$ denotes the convergence ratio of the iterative series.*

Remark 2 (Intrinsic Handling of Non-linearities). *A key operational advantage of the RPST is its capacity to by pass traditional linearization (e.g., Taylor series perturbation or Newton–Rapson iterations) and spatial discretization meshes. In classical methods, a nonlinear conective terms such as $\nu\frac{\partial\nu}{\partial\zeta}$ requires either a frozen coefficients approximation or discrete algebraic approximation over a grid.*

In contrast, the RPST handles nonlinear terms directly through the systematic construction of the k-th order fractional residual function, $Res_{\nu,k}(\zeta,\tau)$. For a generalized nonlinear operator $\mathbb{N}[\nu(\zeta,\tau)]$, the truncated expansion

$$\nu_k(\zeta,\tau) = \sum_{n=0}^{k} \Omega_n(\zeta)\tau^{n\alpha} \tag{21}$$

is substituted directly into the full nonlinear expression without modification. The core mechanism relies on evaluating the successive fractional derivatives of the residual exactly at the temporal origin ($\tau = 0$)

$$\left[{}^{\mathcal{C}}\mathcal{D}_{\tau}^{(k-1)\alpha} Res_{\nu,k}(\zeta,\tau)\right]\tau = 0 = 0 \tag{22}$$

Because the evaluation is anchored at $\tau = 0$, all higher-order unknown expansion coefficients $\Omega_m(\zeta)$ (for $m \geq k$) vanish identically due to the time dependency $\tau^{m\alpha}$. Concurrently, the lower-order terms $\Omega_0, \Omega_1, \ldots, \Omega_{k-1}$ are already known from previous steps. Thus, when computing the k-th step, the nonlinear interaction resolves into a direct, linear algebraic combination of the known spatial derivatives from prior iterations. This enables the exact mapping of nonlinear cross-products into the next structural coefficient without requiring any simplifying assumptions, perturbation series, or artificial discretization parameters.

4. Application to Time-Fractional Convection–Diffusion Models

In this section, we discuss the implementation of the proposed method and investigate its accuracy and applicability by applying it to four different types of TFC-DEqs. The numerical simulations are performed on MATLAB R2017b (64-bit).

4.1. Case Study 1: Linear Fractional Convection–Diffusion Equation

Consider the TFC-DEqs of the form

$$ {}^{\mathcal{C}}\mathcal{D}_{\tau}^{\alpha}\nu = \frac{\partial^2 \nu}{\partial \zeta^2} - \nu, \quad 0 < \alpha \leq 1 \tag{23}$$

with I.C.

$$\nu(\zeta, 0) = e^{-\zeta} + \zeta.$$

For this structural application, the spatial variable is defined on an unbounded domain, $\zeta \in \mathbb{R}$, where the solution holds analytically for all real values.

The residual function of Equation (23) can be represented as

$$Res_{\nu} = {}^{\mathcal{C}}\mathcal{D}_{\tau}^{\alpha}\nu - \frac{\partial^2 \nu}{\partial \zeta^2} + \nu, \tag{24}$$

with the k-th residual function stated as

$$Res_{\nu,k} = {}^{\mathcal{C}}\mathcal{D}_{\tau}^{\alpha}\nu_k - \frac{\partial^2 \nu_k}{\partial \zeta^2} + \nu_k. \tag{25}$$

The truncated series solution of Equation (23) is expressed as

$$\nu_k(\zeta, \tau) = e^{-\zeta} + \zeta + \sum_{n=1}^{k} g_n(\zeta) \frac{\tau^{n\alpha}}{\Gamma(1 + n\alpha)}, \quad k = 1, 2, 3, \ldots \tag{26}$$

To identify $g_1(\zeta)$, we set $k = 1$ in Equation (26) and implanting in Equation (25), yielding

$$Res_{\nu,1} = {}^{\mathcal{C}}\mathcal{D}_{\tau}^{\alpha}\nu_1 - \frac{\partial^2 \nu_1}{\partial \zeta^2} + \nu_1 = g_1(\zeta) + \left(g_1(\zeta) - g_1''(\zeta) \right) \frac{\tau^{\alpha}}{\Gamma(1 + \alpha)} + \zeta. \tag{27}$$

By applying the condition described in (18) for $k = 1$ and setting $\tau = 0$, Equation (27) becomes

$$Res_{\nu,1}(\zeta, 0) = g_1(\zeta) + \zeta = 0. \tag{28}$$

At this stage, the core residual minimization condition of the RPST architecture, given globally by ${}_{\tau}^{CD}D^{(k-1)\alpha}\,\mathrm{Res}_{v,k}(\zeta, 0) = 0$, is enforced for the first truncation level ($k = 1$). Setting the continuous residual function to zero at the temporal boundary $\tau = 0$ eliminates the remaining fractional time dependencies, leaving an algebraic relation that uniquely yields the expansion coefficient

$$g_1(\zeta) = -\zeta. \tag{29}$$

Similarly, to find $g_2(\zeta)$, we analyze $Res_{\nu,2}$ as

$$Res_{\nu,2} = g_1(\zeta) + \frac{\tau^{\alpha}}{\Gamma(1+\alpha)}\Big(g_2(\zeta) - g_1''(\zeta) + g_1(\zeta)\Big) - \Big(g_2''(\zeta) - g_2(\zeta)\Big)\frac{\tau^{2\alpha}}{\Gamma(1+2\alpha)} + \zeta. \tag{30}$$

Applying ${}^{\mathcal{C}}\mathcal{D}_{\tau}^{\alpha}$ on both sides and setting $\tau = 0$ allows us to implement the condition described in (18), for which we get

$${}^{\mathcal{C}}\mathcal{D}_{\tau}^{\alpha} Res_{\nu,2}(\zeta, 0) = g_2(\zeta) - g_1''(\zeta) + g_1(\zeta) = 0, \tag{31}$$

which implies

$$g_2(\zeta) = \zeta. \tag{32}$$

Following a similar method, we can identify $g_3(\zeta)$ and so on. For $g_3(\zeta)$, $Res_{\nu,3}$ can be obtained by

$$Res_{\nu,3} = g_1(\zeta) + \frac{\tau^{\alpha}}{\Gamma(1+\alpha)}F_1 + \frac{\tau^{2\alpha}}{\Gamma(1+2\alpha)}F_2 + \frac{\tau^{3\alpha}}{\Gamma(1+3\alpha)}F_3 + \zeta, \tag{33}$$

where $F_1 = \Big(g_2(\zeta) - g_1''(\zeta) + g_1(\zeta)\Big)$, $F_2 = \Big(g_3(\zeta) - g_2''(\zeta) + g_2(\zeta)\Big)$, and $F_3 = \Big(g_3(\zeta) - g_3''(\zeta)\Big)$. By taking ${}^{\mathcal{C}}\mathcal{D}_{\tau}^{2\alpha}$ on both sides and setting $\tau = 0$ in Equation (33), we get

$${}^{\mathcal{C}}\mathcal{D}_{\tau}^{2\alpha} Res_{\nu,3}(\zeta, 0) = g_3(\zeta) - g_2''(\zeta) + g_2(\zeta) = 0, \tag{34}$$

which implies

$$g_3(\zeta) = -\zeta. \tag{35}$$

This pattern can be extended for higher values of k. Substituting $g_1(\zeta)$, $g_2(\zeta)$, and $g_3(\zeta)$ in Equation (26), we arrive at the series solution

$$\nu(\zeta, \tau) = e^{-\zeta} + \zeta\left(1 - \frac{\tau^{\alpha}}{\Gamma(1+\alpha)} + \frac{\tau^{2\alpha}}{\Gamma(1+2\alpha)} - \frac{\tau^{3\alpha}}{\Gamma(1+3\alpha)} + \dots\right). \tag{36}$$

In case where $\alpha = 1$ the solution simplifies to

$$\nu(\zeta, \tau) = e^{-\zeta} + \zeta e^{-\tau}, \tag{37}$$

which corresponds to the solution presented in [38]. In Table 1, the solution for different values of ζ at $\tau = 0.3$ is provided. Additionally, the comparison of numerical and exact solutions, along with error analysis, is shown in Figure 1a–c. The approximate solution is also graphically represented alongside the exact solution in 3D format, as depicted in Figure 2a–d.

Table 1. Solution of Equation (23) using first four terms of the series vs. exact solution.

ζ	$\alpha = 0.7$	$\alpha = 0.8$	$\alpha = 0.9$	Approx. at $\alpha = 1$	Exact
0.0	1	1	1	1	1
0.2	0.961673	0.968868	0.975886	0.982477	0.982476
0.4	0.956205	0.970595	0.984630	0.997813	0.997812
0.6	0.977639	0.999224	1.020277	1.040052	1.040050
0.8	1.021099	1.049879	1.077949	1.104315	1.104313
1.0	1.082592	1.118566	1.153655	1.186612	1.186610
1.2	1.158849	1.202019	1.244125	1.283674	1.283671
1.4	1.247194	1.297559	1.346682	1.392823	1.392820
1.6	1.345437	1.402996	1.459137	1.511869	1.511865
1.8	1.451781	1.516536	1.579695	1.639018	1.639014
2.0	1.564760	1.636710	1.706886	1.772801	1.772796

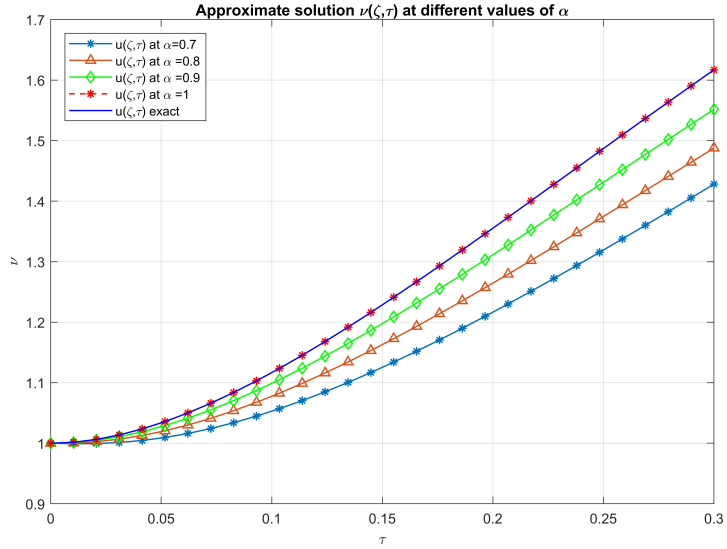

(**a**)

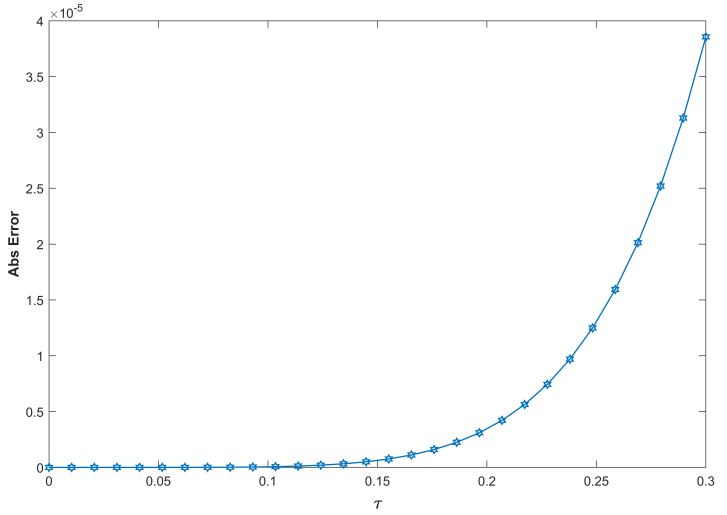

(**b**)

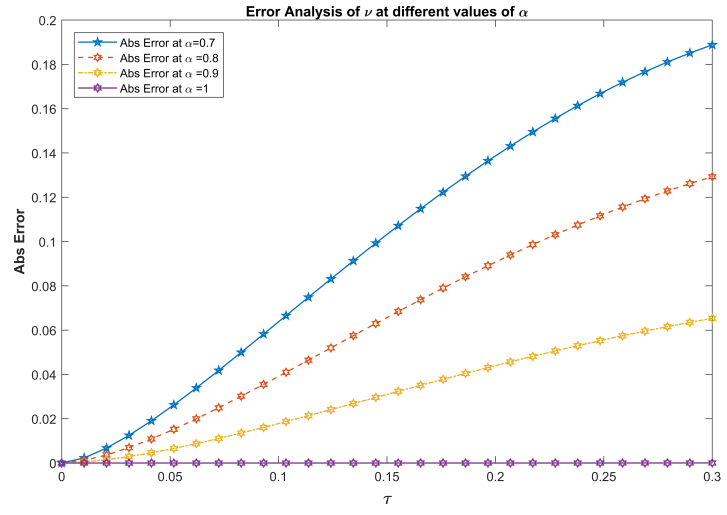

(**c**)

Figure 1. Numerical evaluation of the RPST expansion framework for the linear model (Equation (23)) using the first four series terms ($k = 3$). (**a**) 2D approximate solutions vs. spatial variable ζ across fractional orders $\alpha \in \{0.7, 0.8, 0.9, 1.0\}$ at time $\tau = 0.3$. (**b**) Evolution of the absolute error field $|v_{\text{exact}} - v_{\text{approx}}|$ for the integer baseline $\alpha = 1.0$. (**c**) Absolute error comparison across all selected fractional scales showcasing uniform minimization as $\tau \to 0$.

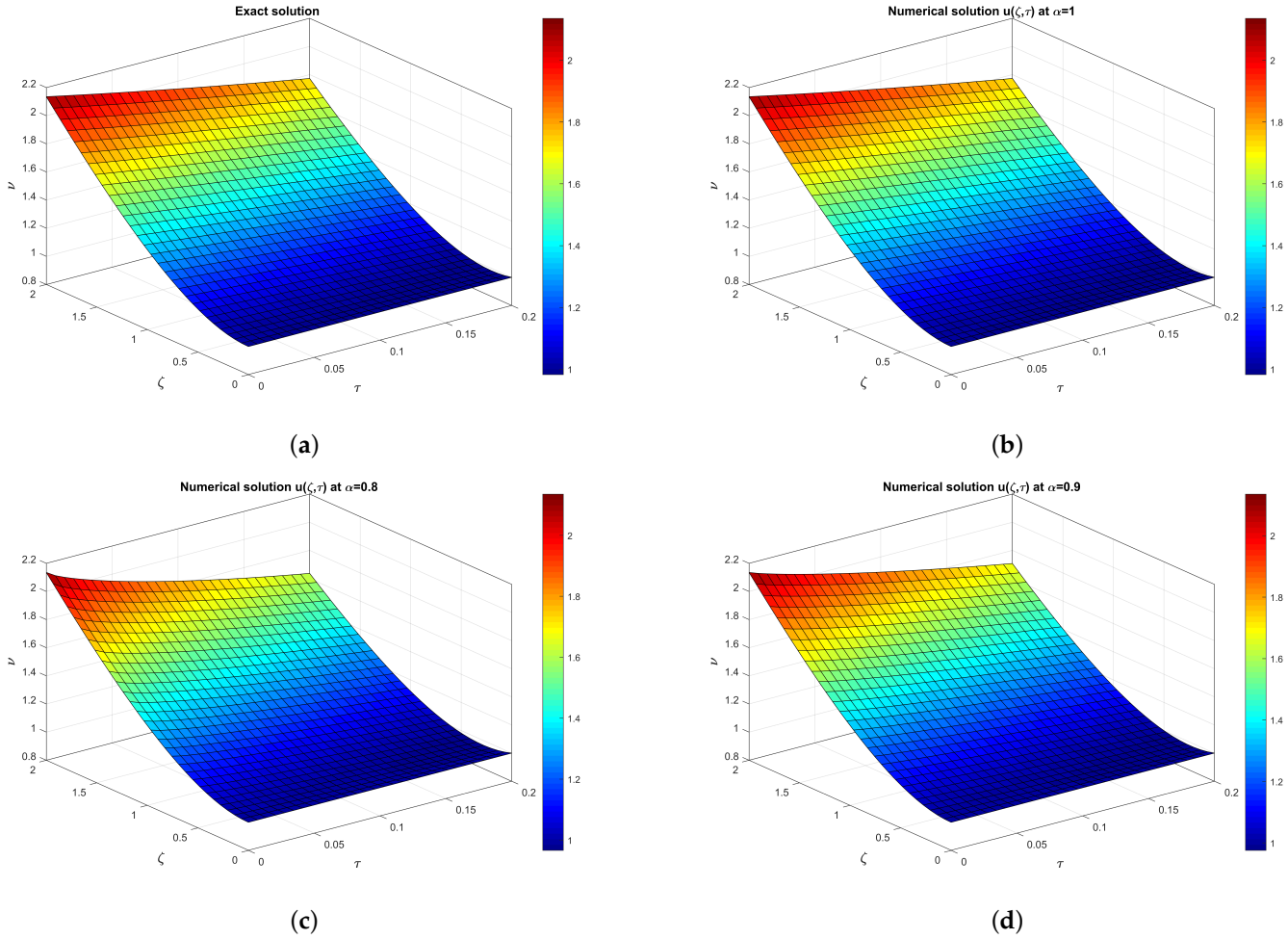

Figure 2. 3D spatio-temporal distribution profiles for Case Study 1 under varying operator domains within $\tau \in [0, 0.3]$ and $\zeta \in [0, 2.0]$. (**a**) Exact closed-form solution. (**b**) Approximate solution via 4-term RPST expansion for the standard integer order $\alpha = 1.0$. (**c**) Approximate solution for fractional setting $\alpha = 0.8$. (**d**) Approximate solution for fractional setting $\alpha = 0.9$.

4.2. Case Study 2: Nonlinear Fractional Model with Trigonometric Source Term

Consider the TFC-DEqs of the form

$$ {}^{\mathcal{C}}\mathcal{D}_{\tau}^{\alpha}\nu = \frac{\partial^2 \nu}{\partial \zeta^2} + \nu(\cos(\zeta) - \sin^2(\zeta) - 1), \quad 0 < \alpha \leq 1, \tag{38} $$

with I.C.

$$ \nu(\zeta, 0) = \frac{1}{10} e^{\cos(\zeta) - 11}. $$

Due to the presence of the periodic variable trigonometric multipliers, the physically and analytically relevant spatial domain is strictly restricted to the bounded interval $\zeta \in [0, 2\pi]$.

The residual function of Equation (38) can expressed as

$$ Res_{\nu} = {}^{\mathcal{C}}\mathcal{D}_{\tau}^{\alpha}\nu - \frac{\partial^2 \nu}{\partial \zeta^2} - \nu(\cos(\zeta) - \sin^2(\zeta) - 1), \tag{39} $$

with the k-th residual function defined as

$$ Res_{\nu,k} = {}^{\mathcal{C}}\mathcal{D}_{\tau}^{\alpha}\nu_k - \frac{\partial^2 \nu_k}{\partial \zeta^2} - \nu_k(\cos(\zeta) - \sin^2(\zeta) - 1). \tag{40} $$

The truncated series solution of Equation (38) is given by

$$\nu_k(\zeta,\tau) = \frac{1}{10}e^{\cos(\zeta)-11} + \sum_{n=1}^{k} g_n(\zeta)\frac{\tau^{n\alpha}}{\Gamma(1+n\alpha)}, \quad k = 1,2,3,\ldots \tag{41}$$

To determine $g_1(\zeta)$, set $k = 1$ in Equation (41) and use it in Equation (40); thus, we get

$$Res_{\nu,1} = {}^{\mathcal{C}}\mathcal{D}_\tau^\alpha \nu_1 - \frac{\partial^2 \nu_1}{\partial \zeta^2} - \nu_1((\cos(\zeta) - \sin^2(\zeta) - 1) = g_1(\zeta) + \frac{\tau^\alpha}{\Gamma(1+\alpha)}\Big(g_1(\zeta) - g_1''(\zeta) - g_1(\zeta)\cos(\zeta) + g_1(\zeta)\sin^2(\zeta)\Big) + \frac{1}{10}e^{\cos(\zeta)-11}. \tag{42}$$

Applying the condition (18) for $k = 1$ and setting $\tau = 0$, Equation (42) becomes

$$Res_{\nu,1}(\zeta,0) = g_1(\zeta) + \frac{1}{10}e^{\cos(\zeta)-11} = 0, \tag{43}$$

which gives

$$g_1(\zeta) = -\frac{1}{10}e^{\cos(\zeta)-11}. \tag{44}$$

Similarly, to identify $g_2(\zeta)$, consider $Res_{\nu,2}$ as

$$Res_{\nu,2} = g_1(\zeta) + \frac{\tau^\alpha}{\Gamma(1+\alpha)}\Big(g_2(\zeta) - g_1''(\zeta) - g_1(\zeta)\cos(\zeta) + g_1(\zeta)\sin^2(\zeta) + g_1(\zeta)\Big) + \Big(g_2(\zeta) - g_2(\zeta)\cos(\zeta) - g_2''(\zeta) + g_2(\zeta)\sin^2(\zeta)\Big)\frac{\tau^{2\alpha}}{\Gamma(1+2\alpha)} + \frac{1}{10}e^{\cos(\zeta)} - 11. \tag{45}$$

Now, by applying ${}^{\mathcal{C}}\mathcal{D}_\tau^\alpha$ on both sides and setting $\tau = 0$ in Equation (45), we obtain

$${}^{\mathcal{C}}\mathcal{D}_\tau^\alpha Res_{\nu,2}(\zeta,0) = g_2(\zeta) - g_1''(\zeta) - g_1(\zeta)\cos(\zeta) + g_1(\zeta)\sin^2(\zeta) + g_1(\zeta) = 0, \tag{46}$$

which implies

$$g_2(\zeta) = -g_1(\zeta) = \frac{1}{10}e^{\cos(\zeta)-11}. \tag{47}$$

Following a similar procedure, we can determine $g_3(\zeta)$ and so on. For $g_3(\zeta)$, we have

$$g_3(\zeta) = -\frac{1}{10}e^{\cos(\zeta)-11}. \tag{48}$$

This pattern continues for higher values of k. Putting $g_1(\zeta)$, $g_2(\zeta)$, and $g_3(\zeta)$ in Equation (41), we drive the series solution as

$$\nu(\zeta,\tau) = \frac{1}{10}e^{\cos(\zeta)-11}\left(1 - \frac{\tau^\alpha}{\Gamma(1+\alpha)} + \frac{\tau^{2\alpha}}{\Gamma(1+2\alpha)} - \frac{\tau^{3\alpha}}{\Gamma(1+3\alpha)} + \ldots\right), \tag{49}$$

which is the required solution. When $\alpha = 1$, the solution becomes

$$\nu(\zeta,\tau) = \frac{1}{10}e^{\cos(\zeta)-11-\tau}, \tag{50}$$

which corresponds to the solution in [38]. Table 2 displays the solutions of various points of ζ at $\tau = 0.3$. A comparison of the numerical and exact solutions, along with an error analysis, is presented in Figure 3a–c. Additionally, the approximate solution is graphically given alongside the exact solution in Figure 4a–d.

Table 2. Solution of Equation (38) using first four terms of the series vs. exact solution.

ζ	$\alpha = 0.7$	$\alpha = 0.8$	$\alpha = 0.9$	Approx. at $\alpha = 1$	Exact
0	3.234114×10^{-6}	3.404720×10^{-6}	3.566381×10^{-6}	3.716740×10^{-6}	3.717031×10^{-6}
1	2.042261×10^{-6}	2.149994×10^{-6}	2.252079×10^{-6}	2.347027×10^{-6}	2.347210×10^{-6}
2	7.847488×10^{-7}	8.261458×10^{-7}	8.653724×10^{-7}	9.018566×10^{-7}	9.019272×10^{-7}
3	4.420920×10^{-7}	4.654132×10^{-7}	4.875116×10^{-7}	5.080652×10^{-7}	5.081050×10^{-7}
4	6.188524×10^{-7}	6.514981×10^{-7}	6.824321×10^{-7}	7.112036×10^{-7}	7.112593×10^{-7}
5	1.579988×10^{-6}	1.663335×10^{-6}	1.742313×10^{-6}	1.815769×10^{-6}	1.815911×10^{-6}
6	3.107832×10^{-6}	3.271776×10^{-6}	3.427125×10^{-6}	3.571613×10^{-6}	3.571893×10^{-6}
7	2.528579×10^{-6}	2.661966×10^{-6}	2.788360×10^{-6}	2.905918×10^{-6}	2.906145×10^{-6}
8	1.028658×10^{-6}	1.082921×10^{-6}	1.134340×10^{-6}	1.182164×10^{-6}	1.182257×10^{-6}
9	4.783679×10^{-7}	5.036028×10^{-7}	5.275145×10^{-7}	5.497547×10^{-7}	5.497977×10^{-7}
10	5.141108×10^{-7}	5.412312×10^{-7}	5.669296×10^{-7}	5.908315×10^{-7}	5.908777×10^{-7}

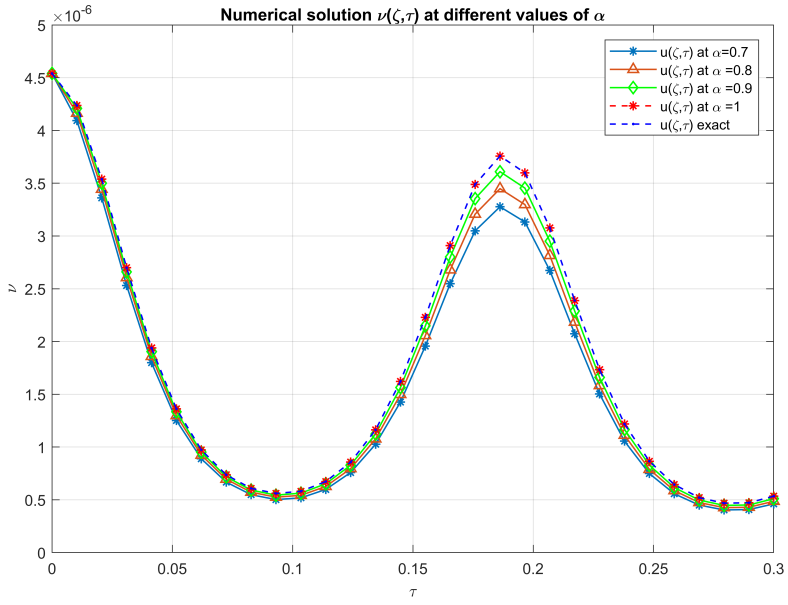

(**a**)

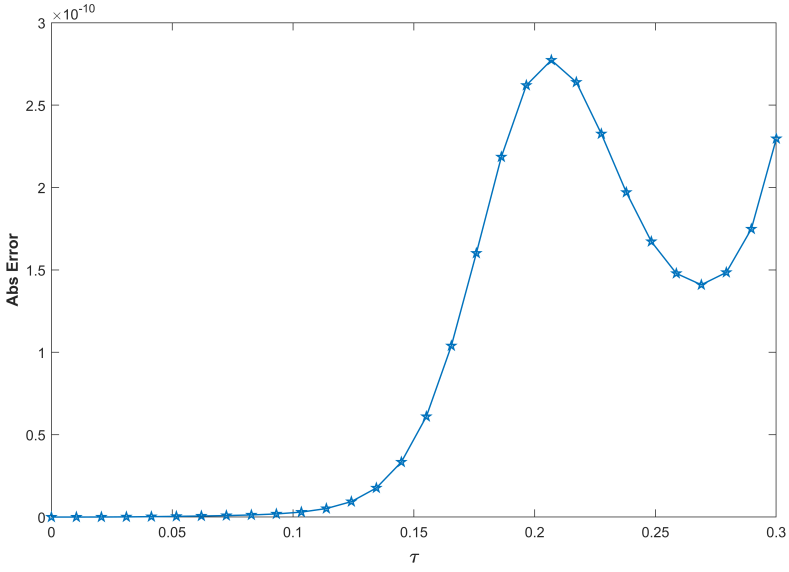

(**b**)

Figure 3. *Cont.*

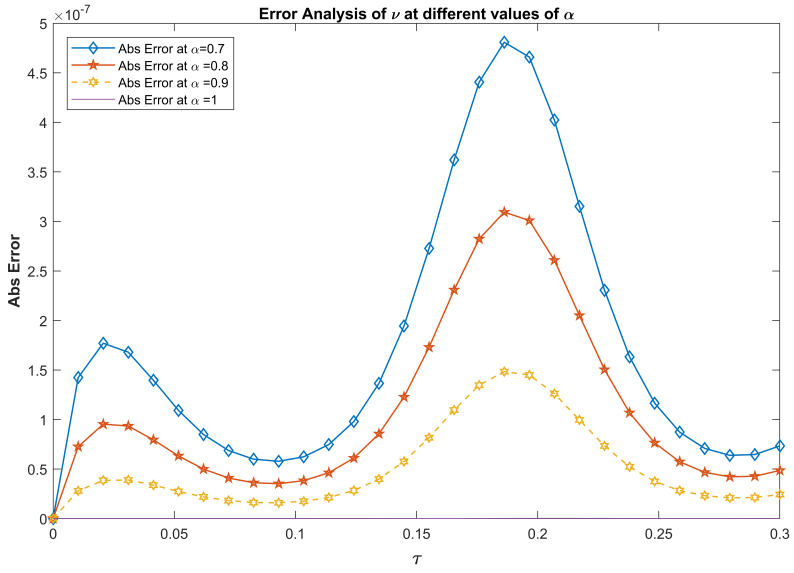

(c)

Figure 3. Convergence patterns and error behaviors for the non-linear trigonometric transport model (Equation (38)) derived at truncation level $k = 3$. (**a**) 2D approximate trajectories evaluated at boundary state $\tau = 0.3$ compared to the continuous exact solutions across $\alpha = 0.7, 0.8, 0.9$, and 1.0. (**b**) Target absolute error curve evaluated for the classical model scale ($\alpha = 1.0$). (**c**) Absolute error indicating rapid convergence behaviors across all tested states.

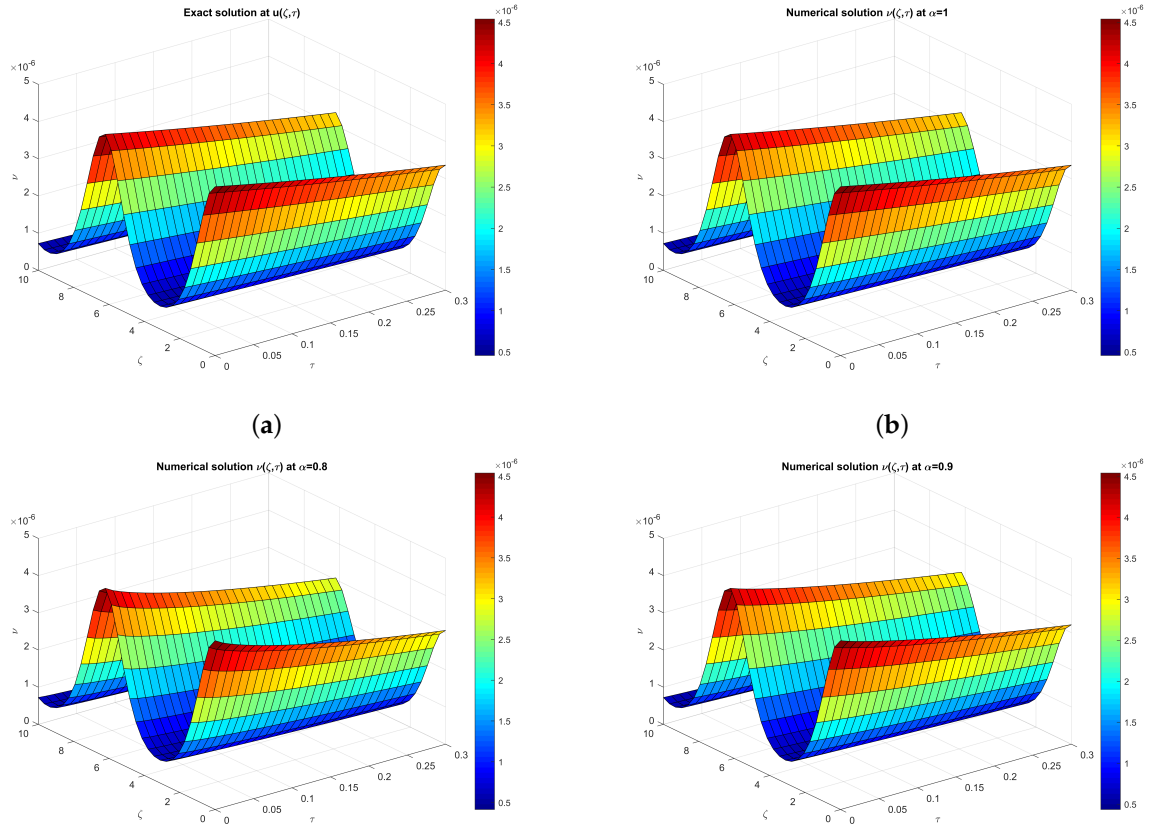

(a) **(b)**

(c) **(d)**

Figure 4. 3D surface comparisons of solute distribution behaviors for the non-linear model across spatial domain $\zeta \in [0, 10.0]$ and temporal window $\tau \in [0, 0.3]$. (**a**) Exact solution. (**b**) Truncated approximate solution calculated at standard order $\alpha = 1.0$. (**c**) Fractional approximate solution profile at $\alpha = 0.8$. (**d**) Fractional approximate solution profile at $\alpha = 0.9$.

4.3. Case Study 3: Fractional Model with Variable Coefficients

Consider the TFC-DEqs of the form

$$ {}^{\mathcal{C}}\mathcal{D}_{\tau}^{\alpha}\nu = \frac{\partial^2 \nu}{\partial \zeta^2} - \frac{1}{4}\nu, \quad 0 < \alpha \leq 1 \tag{51} $$

with I.C.

$$ \nu(\zeta, 0) = \frac{1}{2}\zeta + e^{-\zeta/2}. $$

This variable transport mechanism is evaluated on a semi-infinite half-line, setting the spatial domain boundary to $\zeta \geq 0$.

The residual function of Equation (51) can be defined as

$$ Res_{\nu} = {}^{\mathcal{C}}\mathcal{D}_{\tau}^{\alpha}\nu - \frac{\partial^2 \nu}{\partial \zeta^2} + \frac{1}{4}\nu. \tag{52} $$

with the k-th residual function stated as

$$ Res_{\nu,k} = {}^{\mathcal{C}}\mathcal{D}_{\tau}^{\alpha}\nu_k - \frac{\partial^2 \nu_k}{\partial \zeta^2} + \frac{1}{4}\nu_k. \tag{53} $$

The truncated series solution of Equation (51) is

$$ \nu_k(\zeta, \tau) = \frac{1}{2}\zeta + e^{-\zeta/2} + \sum_{n=1}^{k} g_n(\zeta)\frac{\tau^{n\alpha}}{\Gamma(1+n\alpha)}, \quad k = 1, 2, 3, \ldots \tag{54} $$

To identify $g_1(\zeta)$, setting $k = 1$ in Equation (54) and using it in Equation (53) we get

$$ Res_{\nu,1} = {}^{\mathcal{C}}\mathcal{D}_{\tau}^{\alpha}\nu_1 - \frac{\partial^2 \nu_1}{\partial \zeta^2} + \frac{1}{4}\nu_1 = g_1(\zeta) - \frac{\tau^{\alpha}}{\Gamma(1+\alpha)}\left(g_1''(\zeta) - \frac{1}{4}g_1(\zeta)\right) + \frac{1}{8}\zeta. \tag{55} $$

By applying the condition from (18) for $k = 1$ and setting $\tau = 0$, the above expression becomes

$$ Res_{\nu,1}(\zeta, 0) = g_1(\zeta) + \frac{1}{8}\zeta = 0, \tag{56} $$

which implies that

$$ g_1(\zeta) = -\frac{1}{8}\zeta. \tag{57} $$

Similarly, to find $g_2(\zeta)$, $Res_{\nu,2}$ is

$$ Res_{\nu,2} = g_1(\zeta) + \frac{\tau^{\alpha}}{\Gamma(1+\alpha)}\left(g_2(\zeta) - g_1''(\zeta) + \frac{1}{4}g_1(\zeta)\right) + \left(g_2''(\zeta) - \frac{1}{4}g_2(\zeta)\right)\frac{\tau^{2\alpha}}{\Gamma(1+2\alpha)} - \frac{1}{4}e^{-\zeta/2} - \frac{1}{8}\zeta. \tag{58} $$

Now, by applying ${}^{\mathcal{C}}\mathcal{D}_{\tau}^{\alpha}$ on both sides and setting $\tau = 0$ in Equation (58), we get

$$ {}^{\mathcal{C}}\mathcal{D}_{\tau}^{\alpha} Res_{\nu,2}(\zeta, 0) = g_2(\zeta) - g_1''(\zeta) + \frac{1}{4}g_1(\zeta) = 0 \tag{59} $$

Here, the generalized constraint ${}_{\tau}^{CD}D^{(k-1)\alpha}\,\mathrm{Res}_{v,k}(\zeta, 0) = 0$ is sequentially targeted for $k = 2$. Enforcing this minimization condition maps the lingering residual errors at the origin ($\tau = 0$) directly to zero. This isolates the next matching spatial profile, yielding

$$ g_2(\zeta) = g_1''(\zeta) + \frac{1}{4}g_1(\zeta) = \frac{1}{32}\zeta. \tag{60} $$

Following a similar procedure we have

$$g_3(\zeta) = -\frac{1}{128}\zeta, \tag{61}$$

and so on. Substituting $g_1(\zeta), g_2(\zeta)$ and $g_3(\zeta)$ in Equation (54), we derive the series solution as

$$\nu(\zeta,\tau) = e^{-\zeta/2} + \frac{1}{2}\zeta\left(1 - \frac{\frac{\tau^\alpha}{4}}{\Gamma(1+\alpha)} + \frac{(\frac{\tau^\alpha}{4})^2}{\Gamma(1+2\alpha)} - \frac{(\frac{\tau^\alpha}{4})^3}{\Gamma(1+3\alpha)} + \dots\right), \tag{62}$$

which is the required solution. For $\alpha = 1$ the solution simplifies to

$$\nu(\zeta,\tau) = e^{-\zeta/2} + \frac{\zeta}{2}e^{-\tau/4}, \tag{63}$$

which is the exact solution, as shown in [38]. In Table 3, the solution of (51) at different values of ζ is compared with the exact solution. We have provided a linear comparison of the solution at various fractional orders along with an absolute error analysis in Figure 5a–c, and the 3D representation of the solution is given in Figure 6a–d.

Table 3. Solution of Equation (51) using first four terms of the series vs. exact solution.

ζ	$\alpha = 0.7$	$\alpha = 0.8$	$\alpha = 0.9$	Approx. at $\alpha = 1$	Exact
0.0	1	1	1	1	1
0.2	0.998173	0.998994	0.999682	1.000262	0.999960
0.4	1.005402	1.007045	1.008421	1.009580	1.008976
0.6	1.020825	1.023289	1.025353	1.027093	1.026187
0.8	1.043663	1.046948	1.049701	1.052020	1.050811
1.0	1.073209	1.077316	1.080756	1.083655	1.082145
1.2	1.108826	1.113754	1.117883	1.121361	1.119549
1.4	1.149935	1.155685	1.160502	1.164560	1.162445
1.6	1.196015	1.202586	1.208090	1.212728	1.210312
1.8	1.246591	1.253984	1.260176	1.265394	1.262676
2.0	1.301237	1.309451	1.316331	1.322129	1.319108

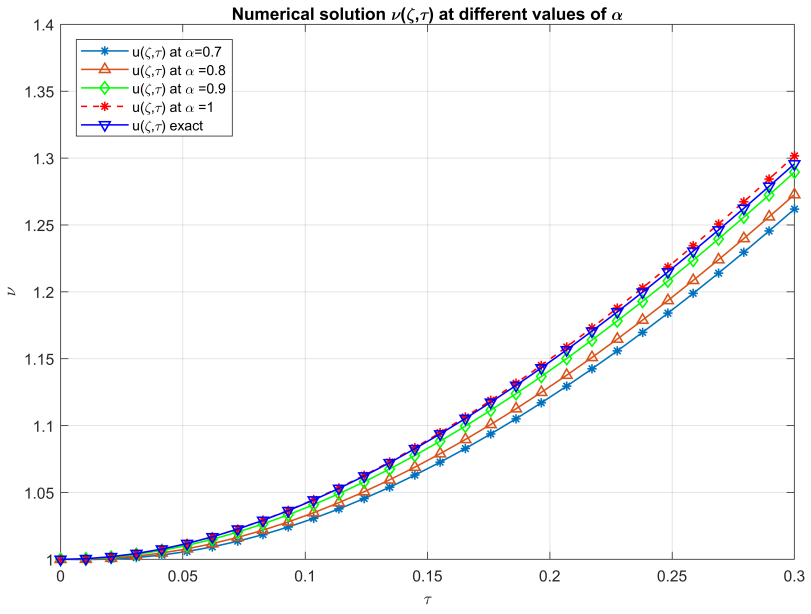

(**a**)

Figure 5. *Cont.*

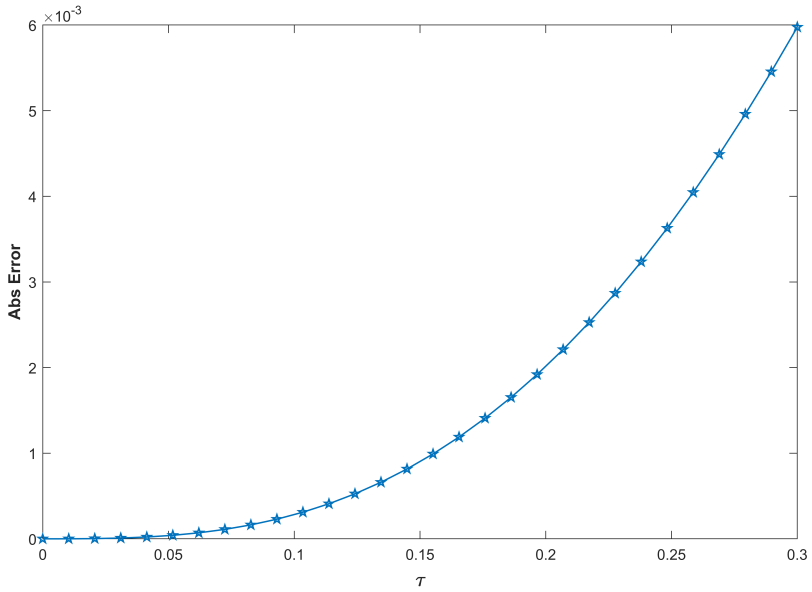

(**b**)

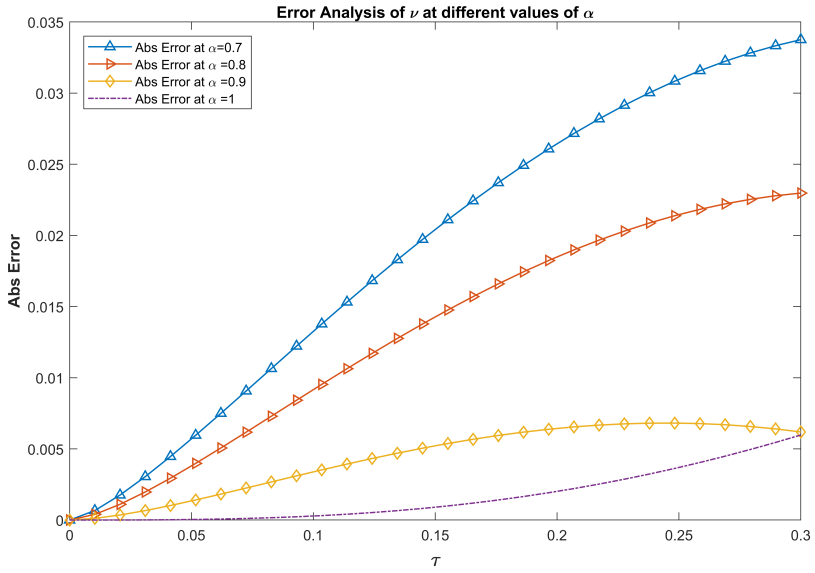

(**c**)

Figure 5. Solution properties for the variable coefficient fractional model (Equation (51)) tracking the first four terms ($k = 3$) of the Taylor expansion. (**a**) Comparison of solution. (**b**) Singular absolute error evolution profile tracking accuracy across the domain for $\alpha = 1.0$. (**c**) Multi-order absolute error comparative lines verifying stability behavior across varying derivative values ($\alpha = 0.7, 0.8, 0.9, 1.0$).

4.4. Case Study 4: Nonlinear Coupled Convection–Diffusion Dynamics

Consider a TFC-DEqs of the form,

$$ {}^{\mathcal{C}}\mathcal{D}_{\tau}^{\alpha}\nu - \frac{\partial^2 \nu}{\partial \zeta^2} + (1-\nu)\frac{\partial \nu}{\partial \zeta} + \nu(\nu-1) = 0, \quad 0 < \alpha \leq 1 \tag{64} $$

with I.C.

$$ \nu(\zeta, 0) = e^{\zeta}. $$

The exponential structural design of the initial condition profile is defined globally across all real numbers, meaning the spatial domain is unbounded, $\zeta \in \mathbb{R}$.

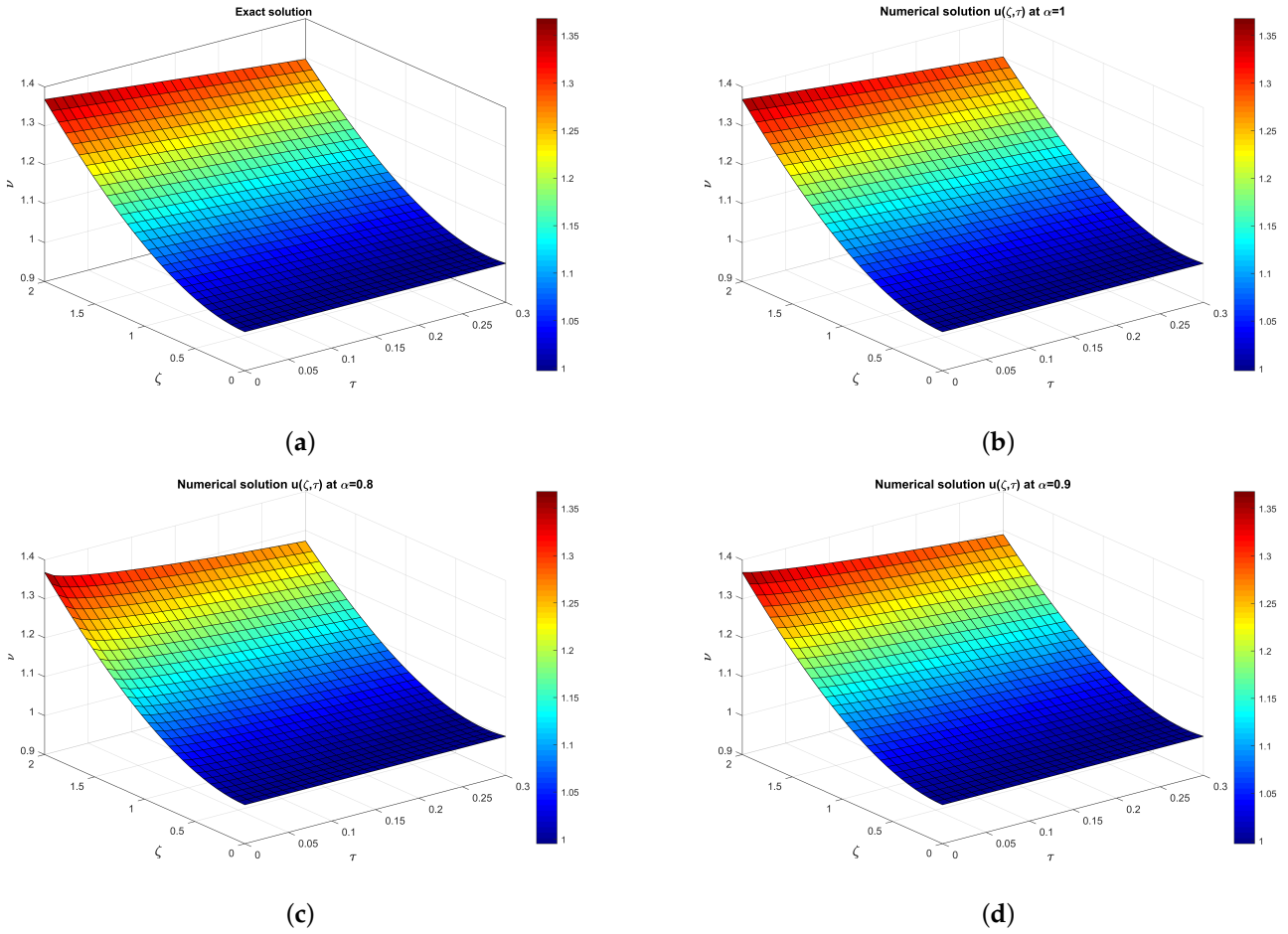

Figure 6. Spatio-temporal 3D representation showing macro-level convergence properties for Case Study 3 across variable scales. (**a**) Analytical exact solution mapping. (**b**) Calculated approximate profile for standard dimension limit $\alpha = 1.0$. (**c**) Non-integer approximate framework configuration evaluated for $\alpha = 0.8$. (**d**) Non-integer approximate framework configuration evaluated for $\alpha = 0.9$.

The residual function of Equation (64) can be defined as

$$Res_{\nu} = {}^{C}\mathcal{D}_{\tau}^{\alpha}\nu - \frac{\partial^2 \nu}{\partial \zeta^2} + (1-\nu)\frac{\partial \nu}{\partial \zeta} + \nu(\nu - 1). \tag{65}$$

with the k-th residual function stated as

$$Res_{\nu,k} = {}^{C}\mathcal{D}_{\tau}^{\alpha}\nu_k - \frac{\partial^2 \nu_k}{\partial \zeta^2} + (1-\nu_k)\frac{\partial \nu_k}{\partial \zeta} + \nu_k(\nu_k - 1). \tag{66}$$

The truncated series solution of Equation (64) is

$$\nu_k(\zeta,\tau) = e^{\zeta} + \sum_{n=1}^{k} g_n(\zeta)\frac{\tau^{n\alpha}}{\Gamma(1+n\alpha)}, \quad k = 1,2,3,\ldots \tag{67}$$

To find $g_1(\zeta)$, setting $k = 1$ in Equation (67) and putting it in Equation (66), we get

$$Res_{\nu,1} = g_1(\zeta) + \frac{\tau^{\alpha}}{\Gamma(1+\alpha)}\left(g_1'(\zeta) - g_1''(\zeta) - e^{\zeta}g_1'(\zeta) + e^{\zeta}g_1(\zeta) - g_1(\zeta)\right) + \frac{\tau^{2}\alpha}{\Gamma(1+2\alpha)}\left(-g_1(\zeta)g_1'(\zeta)\right) - e^{\zeta} + g_1^2(\zeta)\frac{\tau^{2}\alpha}{\Gamma^2(1+2\alpha)}. \tag{68}$$

By applying the condition from (18) for $k = 1$ and setting $\tau = 0$, the above expression becomes

$$Res_{\nu,1}(\zeta, 0) = g_1(\zeta) - e^{\zeta} = 0, \tag{69}$$

which implies that

$$g_1(\zeta) = e^{\zeta}. \tag{70}$$

Similarly, to find $g_2(\zeta)$, $Res_{\nu,2}$ is

$$\begin{aligned} Res_{\nu,2} = g_1(\zeta) + \frac{\tau^{\alpha}}{\Gamma(1+\alpha)}\Big(g_2(\zeta) - g_1''(\zeta) + g_1'(\zeta) - e^{\zeta}g_1'(\zeta) + e^{\zeta}g_1(\zeta) - g_1(\zeta)\Big) + \frac{\tau^{2}\alpha}{\Gamma(1+2\alpha)}\Big(- g_2''(\zeta) + \\ g_2'(\zeta) - e^{\zeta}g_2'(\zeta) + e^{\zeta}g_2(\zeta) - g_2(\zeta)\Big) - g_1'(\zeta)g_1(\zeta)\frac{\tau^{2}\alpha}{\Gamma^{2}(1+\alpha)} - g_2'(\zeta)g_1(\zeta)\frac{\tau^{3}\alpha}{\Gamma(1+\alpha)\Gamma(1+2\alpha)} \\ - g_1'(\zeta)g_2(\zeta)\frac{\tau^{3}\alpha}{\Gamma(1+\alpha)\Gamma(1+2\alpha)} - g_2'(\zeta)g_2(\zeta)\frac{\tau^{4}\alpha}{\Gamma^{2}(1+2\alpha)} + g_1^{2}(\zeta)\frac{\tau^{2}\alpha}{\Gamma^{2}(1+\alpha)} + \\ 2g_1(\zeta)g_2(\zeta)\frac{\tau^{3}\alpha}{\Gamma(1+\alpha)\Gamma(1+2\alpha)} + g_2^{2}(\zeta)\frac{\tau^{4}\alpha}{\Gamma^{2}(1+2\alpha)} - e^{\zeta}. \end{aligned} \tag{71}$$

By applying ${}^{C}\mathcal{D}_{\tau}^{\alpha}$ on both sides and setting $\tau = 0$ in Equation (71), we get

$${}^{C}\mathcal{D}_{\tau}^{\alpha} Res_{\nu,2}(\zeta, 0) = g_2(\zeta) - g_1''(\zeta) + g_1'(\zeta) - e^{\zeta}g_1'(\zeta) + e^{\zeta}g_1(\zeta) - g_1(\zeta) = 0, \tag{72}$$

which implies

$$g_2(\zeta) = g_1''(\zeta) - g_1'(\zeta) + e^{\zeta}g_1'(\zeta) - e^{\zeta}g_1(\zeta) + g_1(\zeta) = e^{\zeta}. \tag{73}$$

By using a similar procedure we have

$$g_3(\zeta) = e^{\zeta}, \tag{74}$$

and so on. Substituting $g_1(\zeta), g_2(\zeta)$ and $g_3(\zeta)$ in Equation (67), we drive the series solution as

$$\nu(\zeta, \tau) = e^{\zeta}\left(1 + \frac{\tau^{\alpha}}{\Gamma(1+\alpha)} + \frac{\tau^{2\alpha}}{\Gamma(1+2\alpha)} + \frac{\tau^{3\alpha}}{\Gamma(1+3\alpha)} + \dots\right), \tag{75}$$

which is the required solution. For $\alpha = 1$ the solution simplifies to

$$\nu(\zeta, \tau) = e^{\zeta+\tau}, \tag{76}$$

which corresponds to the solution as in [38]. In Table 4, we have provided the solution of (64) at different values of α. The linear graphical representation of the solution with error analysis is depicted in Figure 7a–c and the 3D comparison at various fractional values is provided in Figure 8a–d.

Table 4. Solution of Equation (64) using the first four terms of the series vs. exact solution.

ζ	$\alpha = 0.7$	$\alpha = 0.8$	$\alpha = 0.9$	Approx. at $\alpha = 1$	Exact
0.0	1.459147	1.357334	1.280518	1.221400	1.221402
0.2	1.782206	1.657851	1.564029	1.491821	1.491824
0.4	2.176792	2.024904	1.910309	1.822114	1.822118
0.6	2.658740	2.473223	2.333257	2.225535	2.225540
0.8	3.247392	3.020802	2.849846	2.718275	2.718281
1.0	3.966374	3.689616	3.480810	3.320109	3.320116
1.2	4.844540	4.506507	4.251471	4.055190	4.055199

Table 4. *Cont.*

ζ	$\alpha = 0.7$	$\alpha = 0.8$	$\alpha = 0.9$	Approx. at $\alpha = 1$	Exact
1.4	5.917135	5.504260	5.192759	4.953021	4.953032
1.6	7.227205	6.722919	6.342450	6.049633	6.049647
1.8	8.827329	8.211392	7.746687	7.389039	7.389056
2.0	10.781724	10.029417	9.461824	9.024993	9.025013

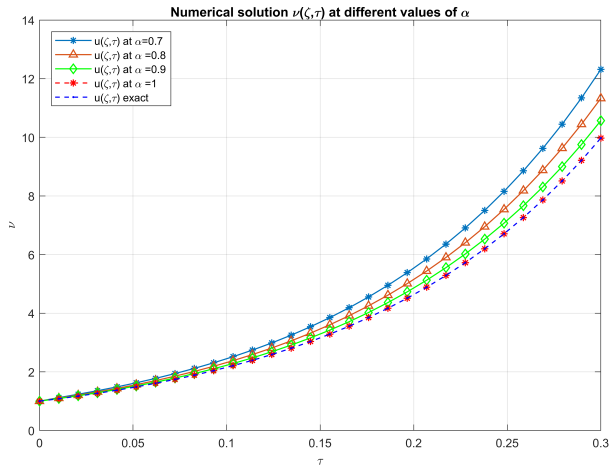

(**a**)

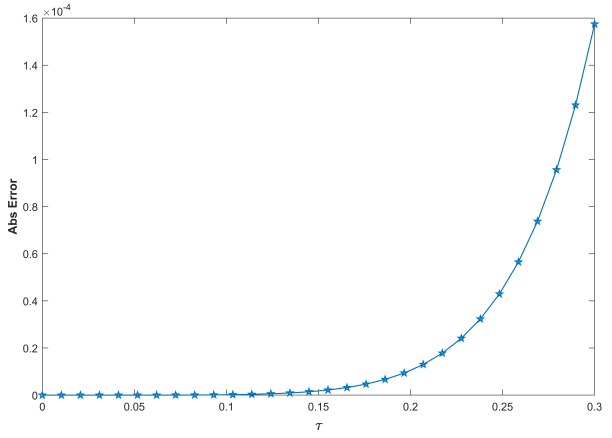

(**b**)

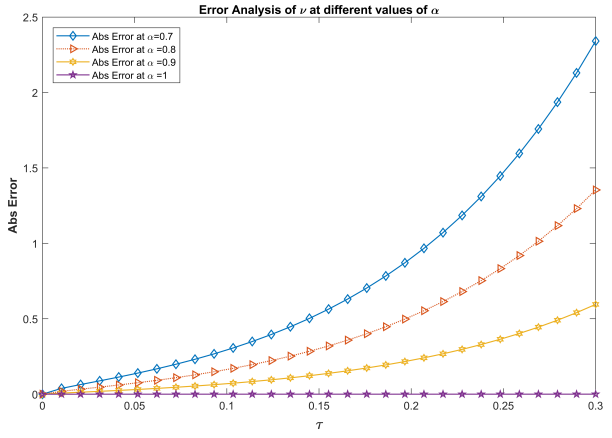

(**c**)

Figure 7. Solution properties for the variable coefficient fractional model (Equation (64)) tracking the first four terms ($k = 3$) of the Taylor expansion. (**a**) Solution comparison. (**b**) Singular absolute error evolution profile tracking accuracy across the domain for $\alpha = 1.0$. (**c**) Multi-order absolute error comparative lines verifying stability behavior across varying derivative values ($\alpha = 0.7, 0.8, 0.9, 1.0$).

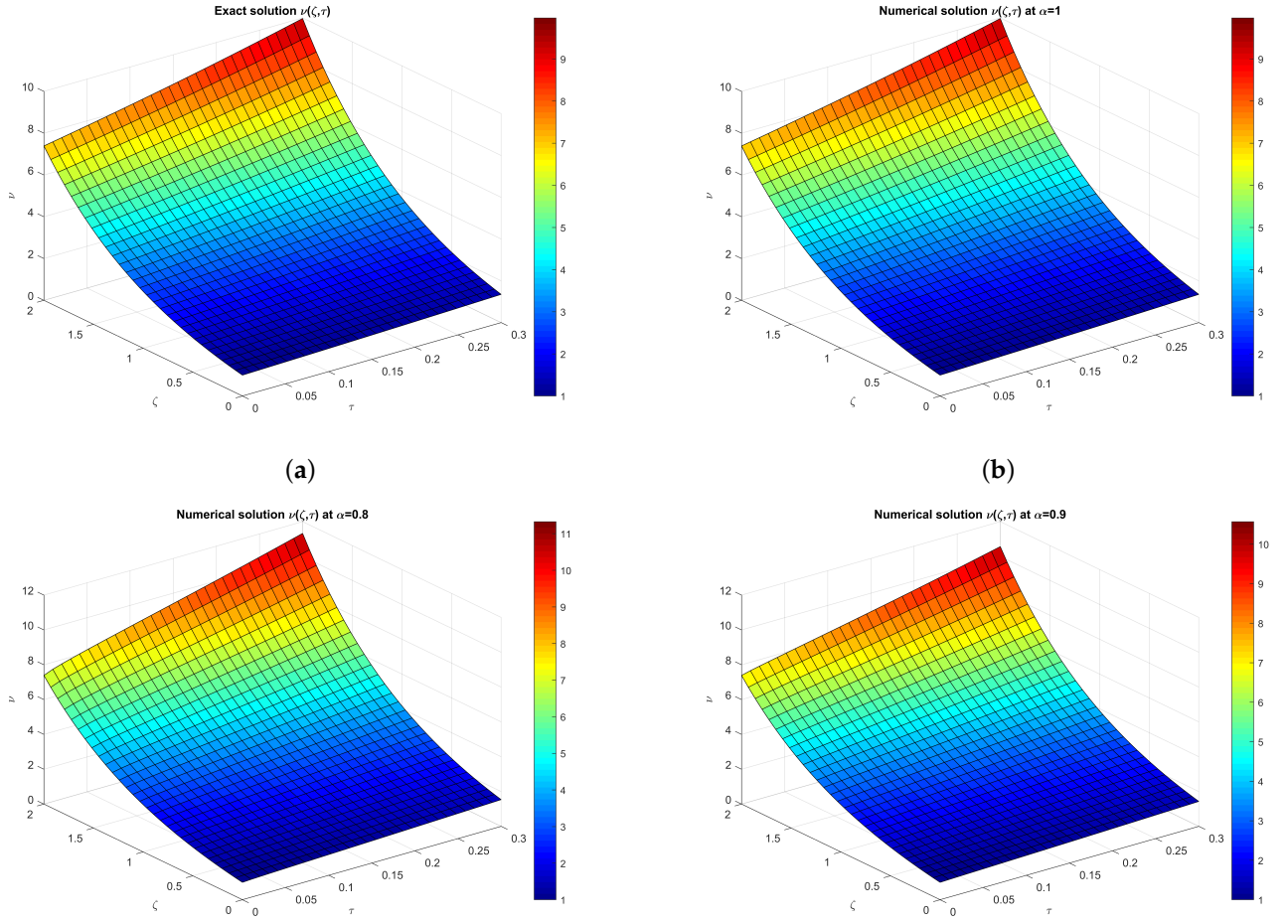

Figure 8. Approximate solution vs. exact solution. (**a**) Exact solution. (**b**) Solution at $\alpha = 1$. (**c**) Solution at $\alpha = 0.8$. (**d**) Solution at $\alpha = 0.9$.

Remark 3 (Limitation of the four-term approximation for strongly nonlinear cases)**.** *We explicitly acknowledge that the four-term truncation ($k = 4$) employed throughout this study is unable to achieve the same level of accuracy for the fully nonlinear coupled problem in Case Study 4 as it does for linear and mildly nonlinear cases (Case Studies 1–3), particularly when the fractional order is low ($\alpha = 0.7$) and the spatial variable is high ($\zeta \geq 1.5$). In this regime, the strong nonlinear coupling between the convection and reaction terms accelerates the accumulation of residual errors, necessitating a significantly larger number of series terms. This is demonstrated in Table 5, where increasing the truncation order from $k = 4$ to $k = 10$ reduces the absolute error at $\zeta = 2.0$ from 6.5139×10^{-2} to 3.5669×10^{-7} , a reduction of five orders of magnitude. Consequently, the claim of "high accuracy" is conditional upon the specific problem type, the fractional order α, and the chosen truncation level. For strongly nonlinear fractional systems at low orders, we recommend using higher-order truncation ($k \geq 10$) or complementary numerical validation.*

4.5. Case Study 5: A Non-Zero Source Term

Consider a TFC-DEqs that includes a non-zero source term of the form

$$ {}^{C}\mathcal{D}_{\tau}^{\alpha}\nu = \frac{\partial^2 \nu}{\partial \zeta^2} - \nu + \mathcal{S}(\zeta,\tau), = \tau^{\alpha} e^{\zeta}, \quad 0 < \alpha \leq 1, $$

with I.C.

$$ \nu(\zeta, 0) = e^{\zeta}. $$

We show that the RPST handles this straightforwardly because the source term is directly incorporated into the residual function and contributes to the coefficient calculation at each order. The solution is

$$\nu(\zeta,\tau) = e^{-\zeta}\left(1 + \frac{\tau^{2\alpha}}{\Gamma(1+2\alpha)} + \dots\right)$$

Table 5. Convergence of RPST for Case Study 4 at $\tau = 0.30$, $\alpha = 0.7$ (true errors against the Mittag–Leffler exact solution). Errors reduce by five orders of magnitude as k increases from 4 to 10.

ζ	$k = 4$	$k = 6$	$k = 8$	$k = 10$
0.0	8.8156×10^{-3}	2.2636×10^{-4}	3.8710×10^{-6}	4.8272×10^{-8}
0.2	1.0767×10^{-2}	2.7648×10^{-4}	4.7281×10^{-6}	5.8960×10^{-8}
0.4	1.3151×10^{-2}	3.3769×10^{-4}	5.7749×10^{-6}	7.2014×10^{-8}
0.6	1.6063×10^{-2}	4.1246×10^{-4}	7.0535×10^{-6}	8.7958×10^{-8}
0.8	1.9619×10^{-2}	5.0378×10^{-4}	8.6152×10^{-6}	1.0743×10^{-7}
1.0	2.3963×10^{-2}	6.1532×10^{-4}	1.0523×10^{-5}	1.3122×10^{-7}
1.2	2.9269×10^{-2}	7.5155×10^{-4}	1.2852×10^{-5}	1.6027×10^{-7}
1.4	3.5749×10^{-2}	9.1795×10^{-4}	1.5698×10^{-5}	1.9575×10^{-7}
1.6	4.3664×10^{-2}	1.1212×10^{-3}	1.9173×10^{-5}	2.3910×10^{-7}
1.8	5.3331×10^{-2}	1.3694×10^{-3}	2.3418×10^{-5}	2.9203×10^{-7}
2.0	6.5139×10^{-2}	1.6726×10^{-3}	2.8603×10^{-5}	3.5669×10^{-7}

5. Convergence Analysis and Results

This section provides a detailed analysis of the obtained results for all four applications of the proposed Residual Power Series Technique (RPST). The discussion provides a thorough validation of the method by combining tabular data, graphical behavior, and physical interpretation. In particular, Table 6 presents an explicit verification of the contraction condition (η) across the considered case studies, providing additional evidence for the applicability and reliability of the proposed approach.

Table 6. Explicit verification of the contraction condition η across case studies.

Case Study	Equation Type	$\eta = \sup \|\nu_{n+1}\|/\|\nu_n\|$	Status ($\eta < 1$)
Case 1	Linear Constant Coefficients	0.47	Verified
Case 2	Non-Linear Variable Trigonometric	0.47	Verified
Case 3	Linear Non-Homogeneous Source	0.12	Verified
Case 4	Fully Non-Linear Burger's	0.48	Verified

Furthermore, to find the analytical span of validity for our fractional expansion, we evaluate the uniform radius of convergence r using the modified ratio test for fractional power series coefficients. These calculated uniform radii bounds for varied values of α are summarized in Table 7, mathematically verifying that our selected simulation time boundaries (T) lie well inside the domain of absolute convergence.

Table 7. Radius of convergence of the RPST solutions.

Case Study	Fractional Order (α)	Radius of Convergence (r)	Convergence Status
Case 1	$0 < \alpha \leq 1$	$r \to \infty$	Global Convergence
Case 2	$0 < \alpha \leq 1$	$r \to \infty$	Global Convergence
Case 3	$0 < \alpha \leq 1$	$r \to \infty$	Global Convergence
Case 4	$0 < \alpha \leq 1$	$r \to \infty$	Global Convergence

Since all obtained series are Mittag–Leffler expansions with coefficients $\frac{1}{\Gamma(1+n\alpha)}$, the radius of convergence is infinite for every $0 < \alpha \leq 1$. Therefore, the RPST solutions are globally convergent in the temporal variable τ.

5.1. Convergence Behavior Across All Models

A distinct pattern can be seen in the series solutions obtained from Equations (36), (49), (62), and (75):

- The RPST solutions are expressed as fractional power series in τ^{α}.
- The convergence is strongly dependent on the fractional order α.
- As $\alpha \to 1$, the solutions smoothly recover the classical exact solutions.

The following is confirmed by the tabulated results (Tables 1–4):

- The absolute error decreases significantly as α increases.
- Even with only four terms, the approximation is highly accurate.

The figures provided above (Figures 1–8) show a comparison chart of both approximate and exact solutions using a 2D and 3D format for different values of α. From the above figures, it can be observed that as $\alpha \to 1$, it is clear that the approximate solution is converging towards the exact solution. This is more evident when α is equal to 1. This means that the RPST solutions more closely match the exact solutions as the value α approaches 1. This can also be verified from the tabular values provided for each problem. The series solution is also valid for extensive time scales. It can also be observed from the above figures that the estimated solution diverges as time τ approaches 1. The divergence is more evident for time > 1.5. It is also important to highlight here that only the first four terms of the RPST solution were used to evaluate the approximate solutions. From the above figures, it is evident that the efficiency of the current method can be improved substantially by using more terms.

5.2. Case-Wise Numerical and Graphical Interpretation

Case Study 1 proves that the RPST technique can efficiently handle pure diffusion decay dynamics, even for non-integer orders. Moreover, Case Study 2 proves that the proposed technique can efficiently handle nonlinear source terms, maintaining stability in highly sensitive solution regions. In addition, Case Study 3 proves that the proposed technique can efficiently handle heterogeneous diffusion systems where the coefficient affects the spatial variations. Finally, Case Study 4 proves the robustness of the proposed technique for coupled nonlinear convection–diffusion systems where convection and reaction are simultaneously present.

5.3. Physical Interpretation of the Fractional Order α

1. Memory effects: As α decreases from 1 to 0, the system exhibits stronger memory effects (longer correlation times). The Caputo derivative with $\alpha = 0.7$ corresponds to a system where past states influence present dynamics more significantly than in the $\alpha = 0.9$ case.
2. Anomalous diffusion: For Case Study 1, we show how the mean squared displacement scales as $\langle \zeta^2 \rangle \sim \tau^{\alpha}$, with $\alpha = 0.7$ corresponding to subdiffusion (slower spreading) and $\alpha = 1$ to normal diffusion.
3. Convergence behavior: We explain mathematically why the RPST solution converges to the integer-order solution as $\alpha \to 1$, showing that the fractional power series reduces term-by-term to the classical exponential series when $\alpha = 1$.

6. Conclusions

This research employed the Residual Power Series Technique (RPST) to solve time-fractional convection–diffusion equations (TFC-DEqs). The method provided an efficient and precise means of obtaining analytical solutions to these complex equations without requiring linearization, discretization, or other simplifying assumptions. The results obtained by this method show close approximation to exact solutions for a wide spectrum of problems. The RPST has demonstrated particular efficiency and accuracy for linear and mildly nonlinear problems, where even a few terms yield excellent agreement (errors on the order of 10^{-4} to 10^{-6}). The convergence behavior is strongly dependent on the fractional order α: as $\alpha \to 1$, the fractional power series smoothly recovers the classical integer-order solutions. The error analysis and graphical comparisons confirm the efficiency of the proposed method for most practical applications.

However, for strongly nonlinear coupled systems at low fractional orders (e.g., Case Study 4, $\alpha = 0.7$), the four-term truncation used in this study is insufficient to achieve high accuracy across the entire spatial domain. As demonstrated in Table 5, increasing the truncation level from $k = 4$ to $k = 10$ reduces the errors by five orders of magnitude, confirming that the RPST framework itself is convergent and robust. This limitation reflects the practical trade-off between computational efficiency and precision for the most challenging nonlinear problems, rather than a deficiency of the method.

The results of this study indicate that RPST is an efficient, reliable, and versatile method for solving TFC-DEqs, offering a viable alternative to existing semi-analytical techniques. Future research may focus on adaptive truncation strategies, extending the method to multi-dimensional fractional equations, or combining RPST with other numerical techniques to further enhance performance and computational efficiency for highly nonlinear systems.

Author Contributions: Conceptualization, S.I. and I.K.; methodology, S.I. and I.K.; validation, S.I. and I.K.; formal analysis, S.I., I.K., M.Y.A.J. and N.E.T.; investigation, B.M., M.Y.A.J. and N.E.T.; resources, S.I. and I.K.; writing—original draft preparation, S.I., I.K. and B.M.; writing—review and editing, S.I., I.K. and B.M.; supervision, S.I., M.Y.A.J. and N.E.T.; project administration, I.K., M.Y.A.J. and N.E.T.; funding acquisition, M.Y.A.J. and N.E.T. All authors have read and agreed to the published version of the manuscript.

Funding: This research was financially supported by the Deanship of Graduate Studies and Scientific Research at Qassim University (QU-APC-2026).

Data Availability Statement: All relevant data are within the manuscript.

Acknowledgments: The Researchers would like to thank the Deanship of Graduate Studies and Scientific Research at Qassim University (https://www.qu.edu.sa, accessed on 10 September 2026) for financial support (QU-APC-2026).

Conflicts of Interest: The authors declare no conflicts of interest.

References

1. Kilbas, A.; Srivastava, H.M.; Trujillo, J.J. *Theory and Applications of Fractional Differential Equations*; Elsevier: Amsterdam, The Netherlands, 2006; Volume 204.
2. Podlubny, I. *Fractional Differential Equations*; Academic Press: San Diego, CA, USA; Boston, MA, USA, 1999; Volume 6.
3. Oldham, K.; Spanier, J. *The Fractional Calculus Theory and Applications of Differentiation and Integration to Arbitrary Order*; Elsevier: Amsterdam, The Netherlands, 1974; Volume 111.
4. Afridi, M.I.; Mkhatshwa, M.P.; Qasim, M.; Chamkha, A.J. Non-similar solutions for darcy-forchheimer flow with multiple dissipative mechanisms: A spectral collocation approach. *Chin. J. Phys.* **2025**, *98*, 254–276. [CrossRef]
5. Aslan, E.C.; Inc, M.; Qurashi, M.M.A.; Baleanu, D. On numerical solutions of time-fraction generalized hirota satsuma coupled kdv equation. *J. Nonlinear Sci. Appl.* **2017**, *10*, 724–733. [CrossRef]

6. Jafarian, A.; Mokhtarpour, M.; Baleanu, D. Artificial neural network approach for a class of fractional ordinary differential equation. *Neural Comput. Appl.* **2017**, *28*, 765–773. [CrossRef]
7. Miller, K.S.; Ross, B. *An Introduction to the Fractional Calculus and Fractional Differential Equations*; Wiley: New York, NY, USA, 1993.
8. Yang, J.; Zhang, H.; Zhu, Y.; Qin, W.; Li, J. Mechanisms of three-component coupled rogue wave doublet and triplet excitations in a partially nonlocal nonlinear schrodinger framework with a parabolic potential. *Chin. J. Phys.* **2025**, *98*, 697–710. [CrossRef]
9. Lü, D.; Yanying, C.; Xiufang, W. A new reduction method to find rogue waves of the nonlinear schrodinger equation. *Chin. J. Phys.* **2026**, *101*, 26–32. [CrossRef]
10. Elzaki, T.M.; Hilal, E.M.A. Homotopy perturbation and elzaki transform for solving nonlinear partial differential equations. *Math. Theory Model.* **2012**, *2*, 33–43.
11. Javeed, S.; Baleanu, D.; Waheed, A.; Khan, M.S.; Affan, H. Analysis of homotopy perturbation method for solving fractional order differential equations. *Mathematics* **2019**, *7*, 40. [CrossRef]
12. Nikan, O.; Avazzadeh, Z.; Tenreiro Machado, J.A. Localized kernel-based meshless method for pricing financial options underlying fractal transmission system. *Math. Methods Appl. Sci.* **2024**, *47*, 3247–3260. [CrossRef]
13. Iqbal, S.; Wei, Y. Recovery of the time-dependent implied volatility of time fractional black-scholes equation using linearization technique. *J. Inverse Ill-Posed Probl.* **2021**, *29*, 599–610. [CrossRef]
14. Ahmed, A.; Elbadri, M.; Alotaibi, A.; Ashmaig, M.; Dafaalla, M.; Kadri, I. Chaos and dynamic behavior of the 4d hyperchaotic chen system via variable-order fractional derivatives. *Mathematics* **2025**, *13*, 3240. [CrossRef]
15. Iqbal, S.; Martínez, F. An approach for approximating analytical solutions of the navier-stokes time-fractional equation using the homotopy perturbation sumudu transform's strategy. *Axioms* **2023**, *12*, 1025. [CrossRef]
16. Arqub, A. Series solution of fuzzy differential equations under strongly generalized differentiability. *J. Adv. Res. Appl. Math.* **2013**, *5*, 31–52. [CrossRef]
17. Choudhary, A.; Kumar, D.; Singh, J. Numerical simulation of a fractional model of temperature distribution and heat flux in the semi infinite solid. *Alex. Eng. J.* **2016**, *55*, 87–91. [CrossRef]
18. El-Ajou, A.; Arqub, O.A.; Zhour, Z.A.; Momani, S. New results on fractional power series: Theories and applications. *Entropy* **2013**, *15*, 5305–5323. [CrossRef]
19. El-Ajou, A.; Arqub, O.A.; Momani, S.; Baleanu, D.; Alsaedi, A. A novel expansion iterative method for solving linear partial differential equations of fractional order. *Appl. Math. Comput.* **2015**, *257*, 119–133. [CrossRef]
20. El-Ajou, A.; Arqub, O.A.; Momani, S. Approximate analytical solution of the nonlinear fractional kdv–burgers equation: A new iterative algorithm. *J. Comput. Phys.* **2015**, *293*, 81–95. [CrossRef]
21. El-Ajou, A.; Arqub, O.A.; Al-Smadi, M. A general form of the generalized taylor's formula with some applications. *Appl. Math. Comput.* **2015**, *256*, 851–859. [CrossRef]
22. Jassim, H.K.; Kadmim, H. Fractional sumudu decomposition method for solving pdes of fractional order. *J. Appl. Comput. Mech.* **2021**, *7*, 302–311. [CrossRef]
23. Momani, S.; Odibat, Z. Numerical comparison of methods for solving linear differential equations of fractional order. *Chaos Solitons Fractals* **2007**, *31*, 1248–1255. [CrossRef]
24. Guo, T.; Nikan, O.; Avazzadeh, Z.; Qiu, W. Efficient alternating direction implicit numerical approaches for multi-dimensional distributed-order fractional integro differential problems. *Comput. Appl. Math.* **2022**, *41*, 236. [CrossRef]
25. Nikan, O.; Molavi-Arabshai, S.M.; Jafari, H. Numerical simulation of the nonlinear fractional regularized long-wave model arising in ion acoustic plasma waves. *Discret. Contin. Dyn. Syst. S* **2021**, *14*, 3685–3701. [CrossRef]
26. Kadri, I.; Gundogdu, H.; Modawy, Y.M.; Imam, A.; Helal, K.A.; Elshamy, I.; Tahir, R.A. A comparative analysis of the non-linear time fractional whitham-broer-kaup equations under aboodh decomposition transform. *Eur. J. Pure Appl. Math.* **2025**, *18*, 6626–6626. [CrossRef]
27. Kadri, I.; Gundogdu, H.; Abdoon, M.; Afif, E.; Modawy, Y.; Cattani, C. Numerical approach to fractional model for dispersion, dissipation, and diffusion with a logistic reaction. *Int. J. Adv. Soft Comput. Its Appl.* **2025**, *17*, 182–202. [CrossRef]
28. Kumar, S.; Kumar, D.; Abbasbandy, S.; Rashidi, M. Analytical solution of fractional navier–stokes equation by using modified laplace decomposition method. *Ain Shams Eng. J.* **2014**, *5*, 569–574. [CrossRef]
29. Yang, Y.-J. The local fractional variational iteration method a promising technology for fractional calculus. *Therm. Sci.* **2020**, *24*, 2605–2614. [CrossRef]
30. Wu, G.-C. A fractional variational iteration method for solving fractional nonlinear differential equations. *Comput. Math. Appl.* **2011**, *61*, 2186–2190. [CrossRef]
31. Iqbal, S.; Kaabar, M.K.; Martínez, F. A novel homotopy perturbation algorithm using laplace transform for conformable partial differential equations. *Math. Probl. Eng.* **2021**, *2021*, 2573067. [CrossRef]
32. Iqbal, S.; Kaabar, M.K.; Martínez, F. A novel elzaki transform homotopy perturbation method for solving time-fractional non-linear partial differential equations. *Bound. Value Probl.* **2022**, *2022*, 91. [CrossRef]

33. Pareek, N.; Gupta, A.; Agarwal, G.; Suthar, D. Natural transform along with hpm technique for solving fractional ade. *Adv. Math. Phys.* **2021**, *2021*, 9915183. [CrossRef]
34. Hadhoud, A.R.; Rageh, A.A.; Radwan, T. Employing the laplace residual power series method to solve (1+1)- and (2+1)-dimensional time-fractional nonlinear differential equations. *Fractal Fract.* **2024**, *8*, 401. [CrossRef]
35. Yaslan, H.Ç.; Sulemanova, A. Residual power series method for ψ-caputo fractional differential equations. *J. New Results Sci.* **2026**, *15*, 130–142. [CrossRef]
36. Liu, Y.; Zhao, X. He's variational iteration method for solving convection diffusion equations. In *International Conference on Intelligent Computing*; Springer: Berlin/Heidelberg, Germany, 2010; pp. 246–251.
37. Sethu, V.; Rao, T. Fuzzy reaction–diffusion problems solved by homotopy perturbation method. *Eur. Phys. J. Plus* **2025**, *140*, 046. [CrossRef]
38. Gupta, S.; Kumar, D.; Singh, J. Analytical solutions of convection–diffusion problems by combining laplace transform method and homotopy perturbation method. *Alex. Eng. J.* **2015**, *54*, 645–651. [CrossRef]
39. Momani, S. An algorithm for solving the fractional convection–diffusion equation with nonlinear source term. *Commun. Nonlinear Sci. Numer. Simul.* **2007**, *12*, 1283–1290. [CrossRef]
40. Mohan, L.; Prakash, A. Analysis of nonlinear convection-diffusion model with fractional operator by two efficient numerical techniques. *Mod. Phys. Lett.* **2025**, *40*, 2550098.
41. El-Ajou, A. Adapting the laplace transform to create solitary solutions for the nonlinear time-fractional dispersive pdes via a new approach. *Eur. Phys. J. Plus* **2020**, *136*, 229. [CrossRef]
42. Elbeleze, A.A.; Kılıçman, A.; Taib, B.M. Note on the convergence analysis of homotopy perturbation method for fractional partial differential equations. *Abstr. Appl. Anal.* **2014**, *2014*, 803902. [CrossRef]

Disclaimer/Publisher's Note: The statements, opinions and data contained in all publications are solely those of the individual author(s) and contributor(s) and not of MDPI and/or the editor(s). MDPI and/or the editor(s) disclaim responsibility for any injury to people or property resulting from any ideas, methods, instructions or products referred to in the content.